Relationship between solar wind, D_{st}, and plasmasphere mass density on one-hour time scales

Victoir Veibell[*]   R.S. Weigel[†]

October 9, 2015

Abstract

This paper compares various magnetosphere conditions around the onset of geomagnetic events, defined as decreases in D_{st} below a threshold value or ρ_{eq} above a threshold value.

1 Introduction

Takahashi et al. [2006] estimated magnetospheric mass density using measurements from the CRRES satellite during a 73-day period and 1991 and found that the average ion mass density, $M = \rho/n_e$, correlated with geomagnetic activity, with lower D_{st} values corresponding to slightly average ion mass densities. They also found a relationship between the average ion mass and 1.5- and 3-day averages of K_p were compared to M. Most measurements occurred in the MLT range of 12:00 and 18:00 in the plasma trough, and CRRES had a nearly equatorial orbit.

Takahashi et al. [2010] developed a mass density dataset using measurements from the GOES satellites over the years 1980 through 1992, with most measurements in the range $L = 6.8 \pm 0.2$. The equatorial mass density, ρ_{eq} was estimated from the estimated mass density using a power law dependence on the geocentric distance to the field line of the observation, R, $\rho = \rho_{eq}L/(R/R_E)$. The mass density ρ was estimated using the the Alfven wave velocity relationship, $V_A = B/\sqrt{\mu_0 \rho}$, a magnetic field model, and a numerical solution to a wave equation with an ionospheric boundary and the assumption of an infinitely conducting ionosphere.

Takahashi et al. [2010] noted that downward spikes in the D_{st} index coincide with with significant changes in ρ_{eq} at an L-shell of 6.8 R_E. For five storms over a 20-day period, two had ρ_{eq} spikes after the D_{st} drop, two had ρ_{eq} spikes before the drop, and one showed little change in ρ_{eq}. A key result was that

when daily-averaged measurements were considered, an enhancment in ρ_{eq} appeared on the same day as minimum D_{st}, indicating the possibility of a solar wind control over ρ_{eq}.

The results of Takahashi et al. [2006] and Takahashi et al. [2010] are consistent with other results on changes in mass density in the plasma trough region. Yao et al. [2008] studied the relationship between D_{st} and ion number density for different ions in different regions (ring current and plasma sheet) and found a general correlation during each of the four storms considered.

? ... ? ....

2 Data Preparation

The parameters ρ_{eq} and $F_{10.7}$ used in this work are from the dataset associated with Denton [2007], with data available from 1980 through 1991; all other parameters are from Kondrashov et al. [2014] over the time range of 1972 through 2013, which are on a 1–hour time grid. ρ_{eq} is the inferred equatorial mass density based on the 3rd harmonic torodial frequency of magnetic field measurements. The smallest cadence for ρ_{eq} values is 10 minutes. To compute an hourly average over the same interval for which the solar wind parameters were averaged, the median of all ρ_{eq} values in a given hourly range was used. Fill values were used for hours in which no measurements were available. In cases where ρ_{eq} was available from multiple Geostationary Operational Environmental Satellites (GOES) satellites at the same time in the Denton [2007] dataset, the value from GOES 6 was selected. In the dataset, measurements

---

[*]vveibell@gmu.edu
[†]rweigel@gmu.edu

from GOES 6 had the longest time span of coverage. An overview of the data is shown in Figure 1.

In this work, events defined to occur when D_{st} or ρ_{eq} crosses a threshold value, as indicated in by horizontal dashed lines in the respective panels of Figure 1. In finding events, all fill values were replaced with linearly interpolated values.

3   Results

Figure 1 shows values of solar wind averages and mass density used in this study.

Figure 2 shows the long-term trends of $log(\rho_{eq})$ and $F_{10.7}$ computed using the median values in 27-day (non-overalpping?) windows using all non–fill hourly values. A scatter plot of these two lines is shown in Figure 2. The linear correlation is found to be 0.94 matching the value found by Takahashi et al. [2010] who used measurements from all satellites in the time interval of 1980 through 1991.

3.1 D_{st} and ρ_{eq} Events

Two types of events are considered. The first is a drop in D_{st} below the threshold of -40 nT. The second is an increase in ρ_{eq} above 40 amu/cm^3.

Our first analysis uses data only from the time interval 1989-1991. For both types of events, the hour of the threshold crossing defines the zero epoch time, and for each event $8 \cdot 24$ hours were kept after each event and $4 \cdot 24$ hours before each event. To compute the epoch averages on a daily time scale, the median value of all measurements for all events centered on a window of ± 12 hours was computed, and these windows were shifted in increments of 24 hours. (Similar results are obtained if we first reduce each event time series to have a 1-day cadence by computing medians in 1-day bins and then compute the medians accross events.) Error bars for each parameter were computed using (2x ?) the standard deviation of the number of values used in computing the median divided by the square root of the number of values used.

In the upper panel of 3, D_{st} events are shown. The minimum D_{st} median is -48 nT. Consistent with Takahashi et al. [2010], D_{st} events correspond to elevated ρ_{eq}, although the magnitude of increase observed here is ~ 2 amu/cm^3 instead of the value of ~ 10 amu/cm^3 found in Takahashi et al. [2010]. The vertical green bars in the ρ_{eq} plot show the number of ρ_{eq} values that were used to compute its median and

error bars. Note that for D_{st}, the number of measurements used in computing the medians is much larger as we use all available D_{st} measurements instead of restricting to only values where a non–fill ρ_{eq} value existed.

In the lower panel of 3, ρ_{eq} events are shown. Here we see that ρ_{eq} enhancements do not clearly correspond to a signature in D_{st}, but that there is a trend for such enhancments to occur when B_z in the IMF is positive. This is consistent with Takahashi et al. [2010] who note that very large increases in ρ_{eq} often corresponded to movement of the plasmasphere to beyond geosynchronous distances.

This method finds 669 such periods between May 1983 and August 1991 with an average duration of 9 hours and a median duration of 3 hours. Figure 5 shows the average values of all events over a window of 24 hours before onset and 48 hours after. Figure 5a shows events selected by looking for event onsets where D_{st} crossed a threshold of -40 nT. The dashed red lines indicate plus and minus one standard deviation of values from all events that went into the average. The final plot in the stack shows both ρ_{eq} and a bar plot of how many valid data points went into the ρ_{eq} average. Since ρ_{eq} comes from a sparser dataset, it has less valid points contributing to the averages than the other parameters in the stack. A subset of longer duration events will be looked at later.

This figure shows a definite spike in the Z component of the magnetic field, as well as the defined drop in D_{st}, but no obvious change in mass density at an hourly timescale. This points to an issue with only looking at long-timescale trends between density and D_{st}, and allows for the possibility that other factors are influencing the long term correlation since there's no obvious connection on a short timescale. One possibility is that, as suggested in Takahashi et al. [2010], $F_{10.7}$ plays a significant role in driving long term density values which biases the long term correlation of density and D_{st}.

Two types of events are considered. The first is a drop in D_{st} below the threshold of -40 nT. The second is an increase in ρ_{eq} above 40 amu/cm^3.

Our first analysis uses data only from the time interval 1989-1991. In this interval, there were (?) D_{st} events and (?) ρ_{eq} events. For both types of events, the hour of the threshold crossing defines the zero epoch time, and for each event $8 \cdot 24$ hours were kept

after each event and $4 \cdot 24$ hours before each event. To compute the epoch averages on a daily time scale, the median value of all measurements for all events centered window of ± 12 hours was computed, and these windows were shifted in increments of 24 hours. (Similar results are obtained if we first reduce each event time series to have a 1-day cadence by computing medians in 1-day bins and then compute the medians accross events.) Error bars for each parameter were computed using the standard deviation of values used in computing the median dividied by the square root of the number of values used.

In the upper panel of 3, D_{st} events are shown. The minimum D_{st} median is -48 nT. Consistent with Takahashi et al. [2010], D_{st} events corrspond to elevated ρ_{eq}, although the magnitude of increase observed here is on the order of ~ 2 amu/cm^3 instead of ~ 10 amu/cm^3 found in Takahashi et al. [2010]. The vertical green bars in the ρ_{eq} plot show the number of ρ_{eq} values that were used to compute its median and error bars. Note that for D_{st}, the number of measurements used in computing the medians is much larger as we use all available D_{st} measurements instead of restricting to only values where a non-fill ρ_{eq} value existed.

In the lower panel of 3, ρ_{eq} events are shown. Here we see that ρ_{eq} enhancements do not clearly correspond to a signature in D_{st}, but that there is a trend for such enhancments to occur when B_z in the IMF is positive. This is consistent with Takahashi et al. [2010] who note that very large increases in ρ_{eq} often corresponded to movement of the plasmasphere to beyond geosynchronous distances.

A total of 669 events were found in the interval of May 1983 through August 1991 with an average duration of 9 hours and a median duration of 3 hours. Figure 5 shows the average values of all events over a window of 24 hours before onset and 48 hours after. Figure 5a shows events selected by looking for event onsets where D_{st} crossed a threshold of -40 nT. The dashed red lines indicate plus and minus one standard deviation of values from all events that went into the average. The final plot in the stack shows both ρ_{eq} and a bar plot of how many valid data points went into the ρ_{eq} average. Since ρ_{eq} comes from a sparser dataset, it has less valid points contributing to the averages than the other parameters in the stack. A subset of longer duration events will be looked at later.

This figure shows a definite spike in the Z component of the magnetic field, as well as the defined drop in D_{st}, but no obvious change in mass density at an hourly timescale. This points to an issue with only looking at long-timescale trends between density and D_{st}, and allows for the possibility that other factors are influencing the long term correlation since there's no obvious connection on a short timescale. One possibility is that, as suggested in Takahashi et al. [2010], $F_{10.7}$ plays a significant role in driving long term density values which biases the long term correlation of density and D_{st}.

3.2 Mass Density Events

Figure 5b shows this same algorithm, but looking for a rise in mass density over a value of 40 amu/cm^3. This results in 130 events with a mean duration of 32 hours and a median duration of 17 hours, marked in red on the left figure.

This shows that when using all data for mass density derived events, almost no significant changes can be seen around event onset.

4   More specific events

It's hypothesized that progressively picking more specific event criteria will allow for the possibility of more significant results, at the expense of more bias in the selection process and potentially less overall usefulness of the results. That said, the predictability of extreme events is of definite interest, so an attempt has been made to find some reproducible method of prediction. Looking at events that last longer than 12 hours and events with an onset threshhold greater than 70g/cm^3 results in the left and right sides of Figure 6 respectively.

Neither of these seem to indicate anything too significant, so looking at D_{st} events instead to look for something that causes a significant change in Mass Density results in Figure 7. This shows that by either looking only at D_{st} events that last longer than an hour (left) or at events where the onset condition is $D_{st} < -80$ nT, a spike in mass density is seen, but also a definite lack of data availability to the point where that spike may be coming from less than five of the total 143 events.

Unfortunately there are no events in this time frame that are longer than 12 hours with D_{st} minima lower than -80 nT that have existing mass density data around onset, so an analysis of this particular relationship can't be made.

Neither of these seem to indicate anything too sig-

nificant, so looking at D_{st} events instead to look for something that causes a significant change in Mass Density results in Figure 7. This shows that by either looking only at D_{st} events that last longer than an hour (left) or at events where the onset condition is $D_{st} < -80$ nT, a spike in mass density is seen, but also a definite lack of data availability to the point where that spike may be coming from less than five of the total 143 events.

Unfortunately there are no events in this time frame that are longer than 12 hours with D_{st} minima lower than -80 nT that have existing mass density data around onset, so an analysis of this particular relationship can't be made.

4.1 Change in ρ_{eq}

Instead of looking for events based on a threshold of ρ_{eq}, we instead looked for a certain amount of change in ρ_{eq} as the basis for event onset. Both raw change and percent change were done in case of bias towards high or low ρ_{eq} periods, respectively, but neither showed any correlation to a change in D_{st}.

5 F10.7 dependence

In an effort to analyze the dependence of ρ_{eq} on $F_{10.7}$, a few tests were performed. Takahashi et al. [2010] mention a strong correlation between the two. The long term correlation could be a bias for D_{st}'s effects, so a linear model was created, recreating mass density purely from $F_{10.7}$ in the form of $\rho_{eq}(t) = A \cdot F_{10.7}(t)$. This re-created ρ_{eq} shows around a 45% correlation with the actual ρ_{eq}, suggesting a strong influence, while doing the same procedure with D_{st} shows only a 20-25% correlation.

Figure 9 takes the events and bins them by the value of $F_{10.7}$ at event onset, then looks at both ρ_{eq} and B_z. Error bars calculated in the same manner as before are added to the highest and lowest bins. A significant difference is seen in ρ_{eq} between events taking place during periods of high $F_{10.7}$ and low $F_{10.7}$, while a much less significant, but still noticeable, difference is seen in B_z. Also of interest is how ρ_{eq} only sharply reacts to D_{st} events during periods of high $F_{10.7}$. The positive relationship seen in Takahashi et al. [2010] could be due to the short time period looked at, and that it coincides with periods of higher $F_{10.7}$.

6 Appendix

6.1 Bias

While attempting to reproduce Figure 11 from Takahashi et al. [2010], an ambiguity in data-handling was found. It is unknown how they got from hourly ρ_{eq} to daily medians, whether in one step or two steps, and whether the hourly medians are an hour ahead of each hour grid point, or a median of points a half hour to either side, so attempts were made to reproduce all possibilities and compare in order to find a data-handling method with the least bias. These attempts are shown in Figure 10. This also shows the effect of only considering events with a minimum before noon. All show a similar spike in ρ_{eq} at the time of D_{st} minimum, though none quite reproduce the exact values seen in Takahashi et al. [2010]. Figure 11 shows where the median falls for all of the found events during that period, as a sanity check for why the prior work would get median values nearing 30 amu/cm^3. Both authors of this paper conducted independent trials to confirm that the data and analysis don't quite yield the results of Figure 11 in Takahashi et al. [2010] with the processes described in that paper, but the same general trend is still seen.

To check for potential bias in the data as used by our analysis, we checked how the data availability varied with hour, shown in Figure 12. We also looked at how storm conditions affected data availability. Both a two sample t-test for difference in means and a Wilcoxon rank sum test showed significance at the 1% level that D_{st} during periods with available data was of a different distribution than D_{st} during periods missing data. When testing for other significant D_{st} differences, the Wilcoxon test was significant while the t-test was not in pre-noon vs post-noon distributions, as well as $\rho_{eq} > 40$ vs $\rho_{eq} < 40$ distributions indicating perhaps an increase in variability without an increase in mean.

While the GOES Satellites tend to keep an average geostationary distance of around $L = 6.8R_E$ shown in Takahashi et al. [2010], the actual plasmapause location varies significantly, as shown in O'Brien and Moldwin [2003]. This means that during periods of large D_{st} the plasmapause may be far from the point of measurement of ρ_{eq} creating a discord in the correlation. Gallagher et al. [2000] provides a model for ρ_{eq} at a range of L-shells and a brief discussion of the elemental contributions.

References

R. Denton. Database of Input Parameters for Tsyganenko Magnetic Field Models, 2007. URL http://www.dartmouth.edu/~rdenton/magpar/index.html.

D. L. Gallagher, P. D. Craven, and R. H. Comfort. Global core plasma model. *Journal of Geophysical Research*, 105:18819, August 2000. doi:10.1029/1999JA000241.

D. Kondrashov, R. Denton, Y. Y. Shprits, and H. J. Singer. Reconstruction of gaps in the past history of solar wind parameters. *Geophysical Research Letters*, 41:2702–2707, April 2014. doi:10.1002/2014GL059741.

T. P. O'Brien and M. B. Moldwin. Empirical plasmapause models from magnetic indices. *Geophysical Research Letters*, 30:1152, February 2003. doi:10.1029/2002GL016007.

K. Takahashi, R. E. Denton, R. R. Anderson, and W. J. Hughes. Mass density inferred from toroidal wave frequencies and its comparison to electron density. *Journal of Geophysical Research (Space Physics)*, 111:A01201, January 2006. doi:10.1029/2005JA011286.

K. Takahashi, R. E. Denton, and H. J. Singer. Solar cycle variation of geosynchronous plasma mass density derived from the frequency of standing Alfvén waves. *Journal of Geophysical Research (Space Physics)*, 115:A07207, July 2010. doi:10.1029/2009JA015243.

Y. Yao, K. Seki, Y. Miyoshi, J. P. McFadden, E. J. Lund, and C. W. Carlson. Effect of solar wind variation on low-energy O+ populations in the magnetosphere during geomagnetic storms: FAST observations. *Journal of Geophysical Research (Space Physics)*, 113, 2008. doi:10.1029/2007JA012681.

7 Figures
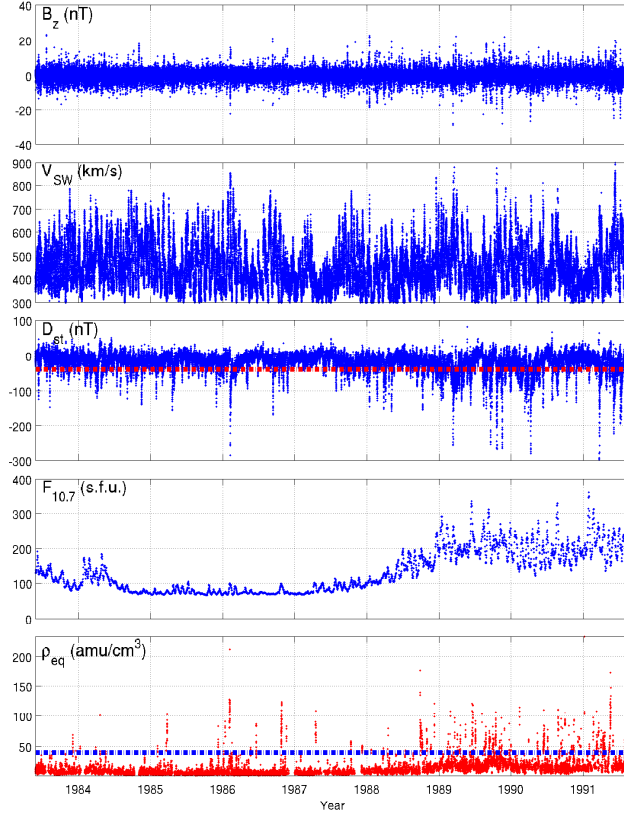
Figure 1: Overview of data used in this study. The top four panels show parameters from Kondrashov et al. [2014] and the bottom panel is based on ρ_{eq} from Denton [2007] after interpolation and averaging described in the text. Dashed horizontal lines in the D_{st} and ρ_{eq} panels indicate sample event cutoff thresholds of $D_{st} = -50$ nT and $\rho_{eq} = 40$ amu/cm^3 .
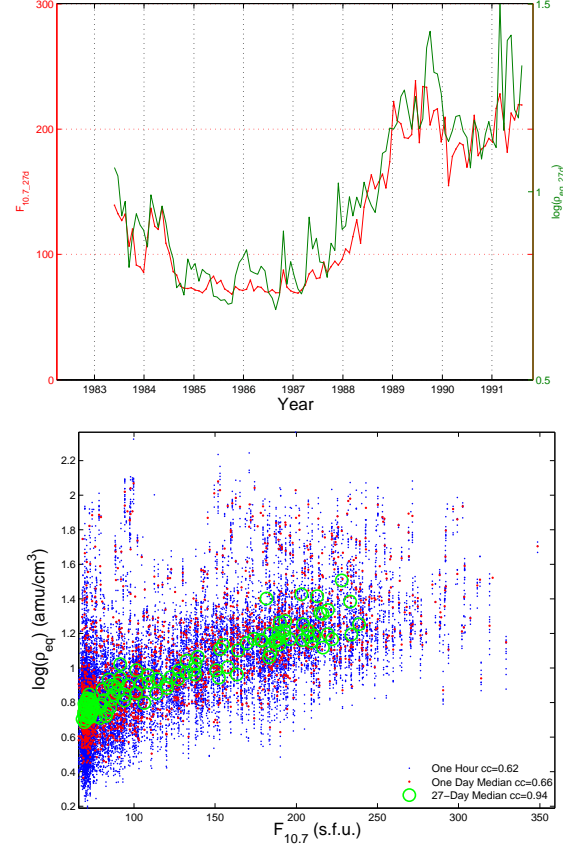
Figure 2: (a) 27-day averages of $F_{10.7}$ and ρ_{eq}. (b) Correlation between $\log(\rho_{eq})$ and $F_{10.7}$ using hour, day, and 27-day averaging intervals; compare to Takahashi et al. [2010] Fig. 14.
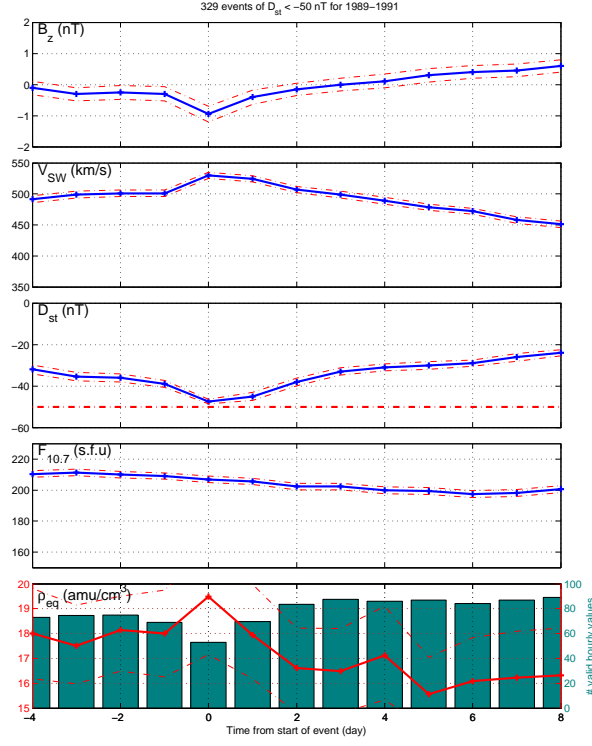
Figure 3: Events in the interval 1989-1991. Upper panel: D_{st} events. Lower panel: ρ_{eq} events.
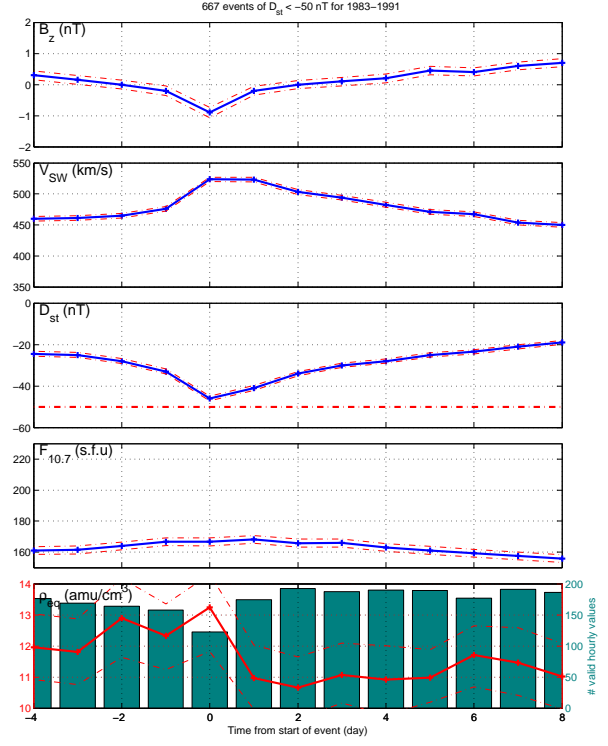
Figure 4: Events in the interval 1983-1991. Upper panel: D_{st} events. Lower panel: ρ_{eq} events.
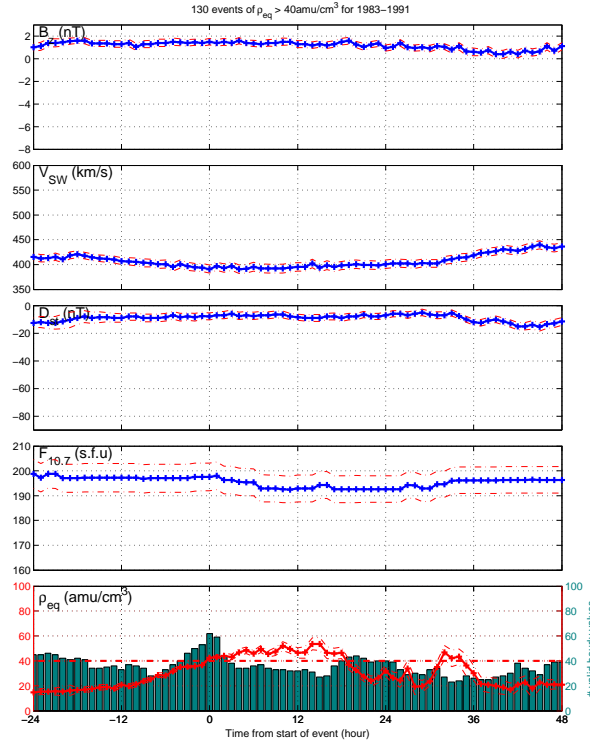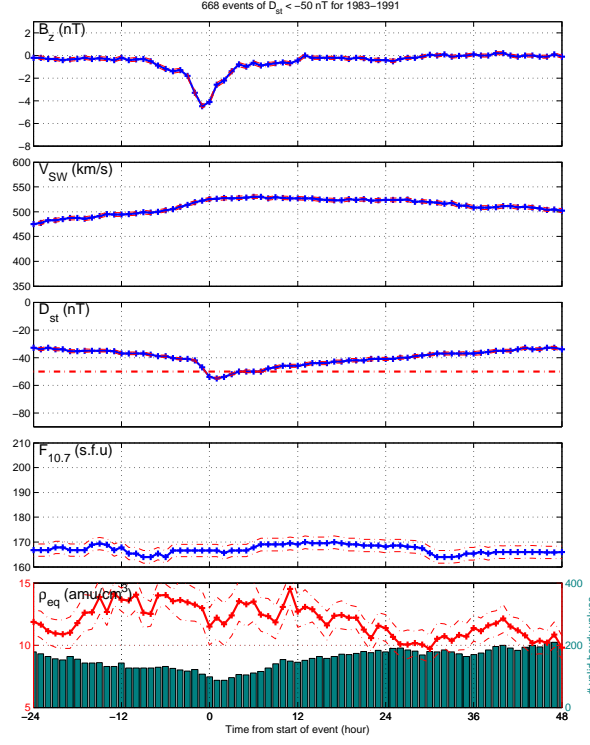
Figure 5: (a) Average of solar wind and near-Earth measurements around the time D_{st} crossed below -50 nT onset. (b) Same as (a) except around time intervals where mass density crossed above 40 amu/cm^3.
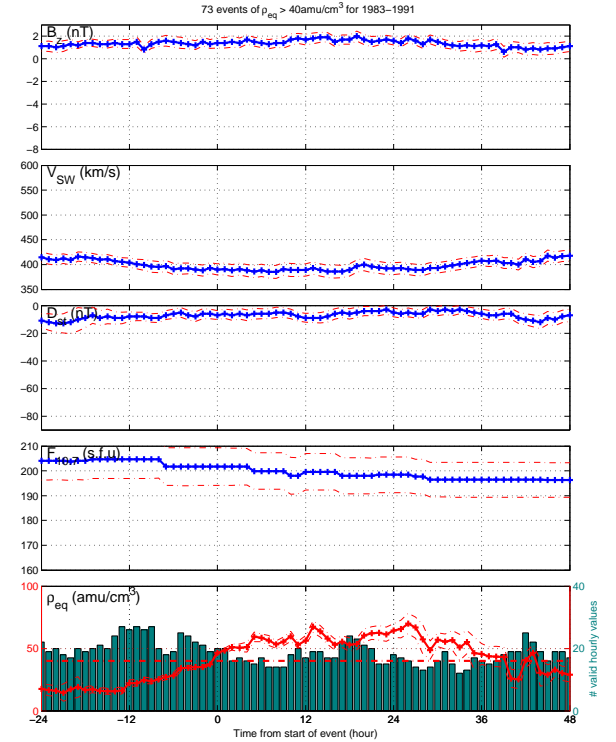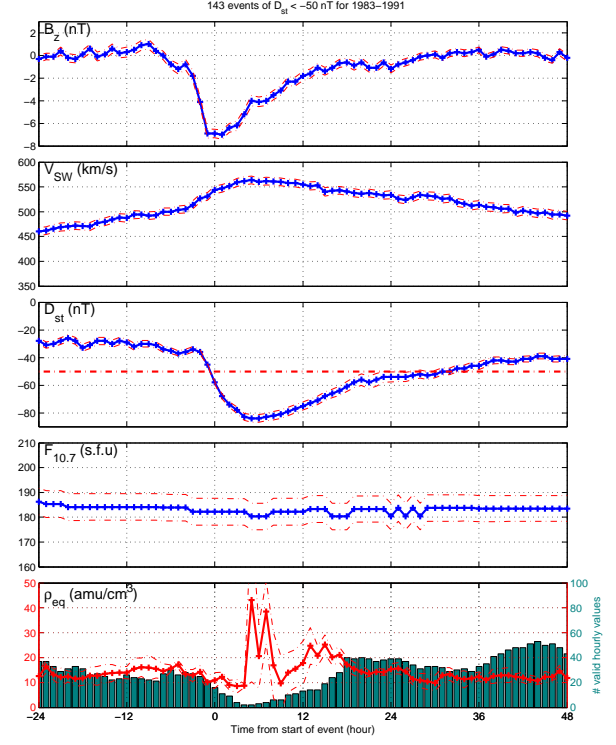
Figure 6: (a) Same as Figure 5(a) except with constraint that D_{st} stayed below -50 nT for at least 12 hours. (b) Same as Figure 5(b) except for constrain that ρ_{eq} stayed above 50 amu/cm^3 for at least 12 hours.
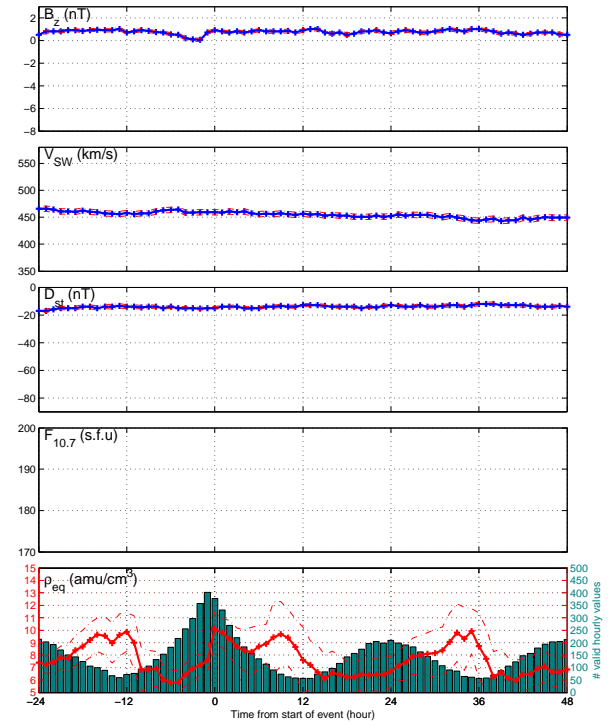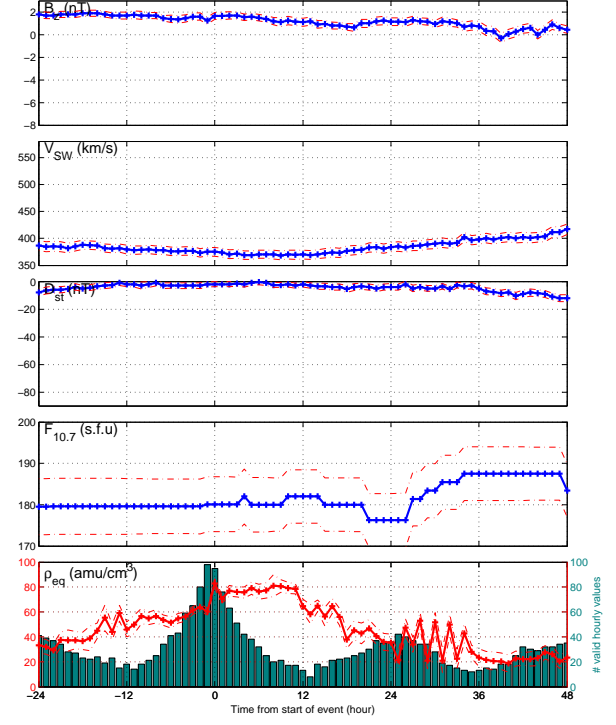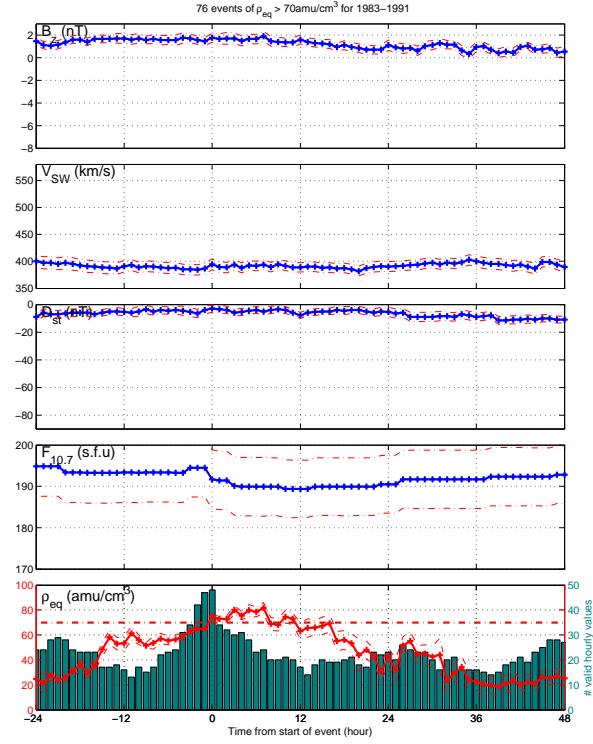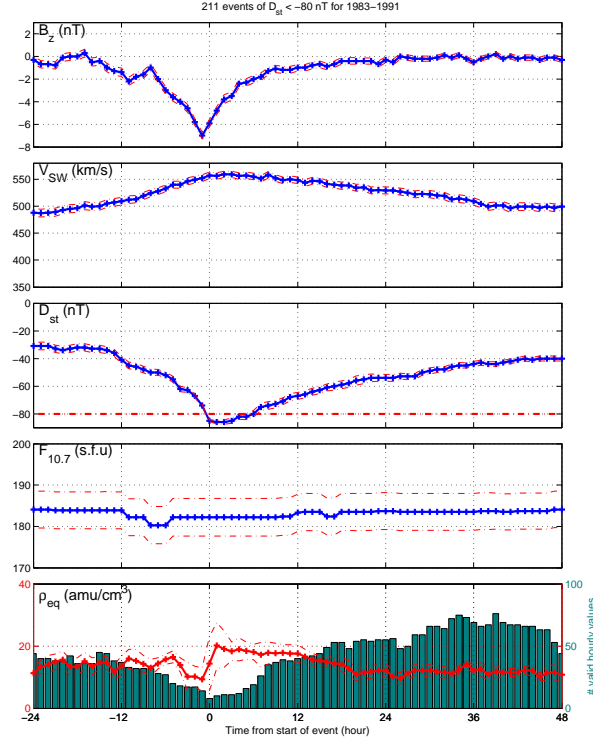
Figure 7: (a) Same as Figure 5(a) except with constraint that D_{st} crossed below -80 nT (b) Same as Figure 5(b) except for constrain that ρ_{eq} crossed above 70 amu/cm^3.

Figure 8: (a) diff(ρ_{eq}) $> 10\frac{amu}{hour}$. (b) diff(ρ_{eq}) $> 30\frac{\%}{hour}$
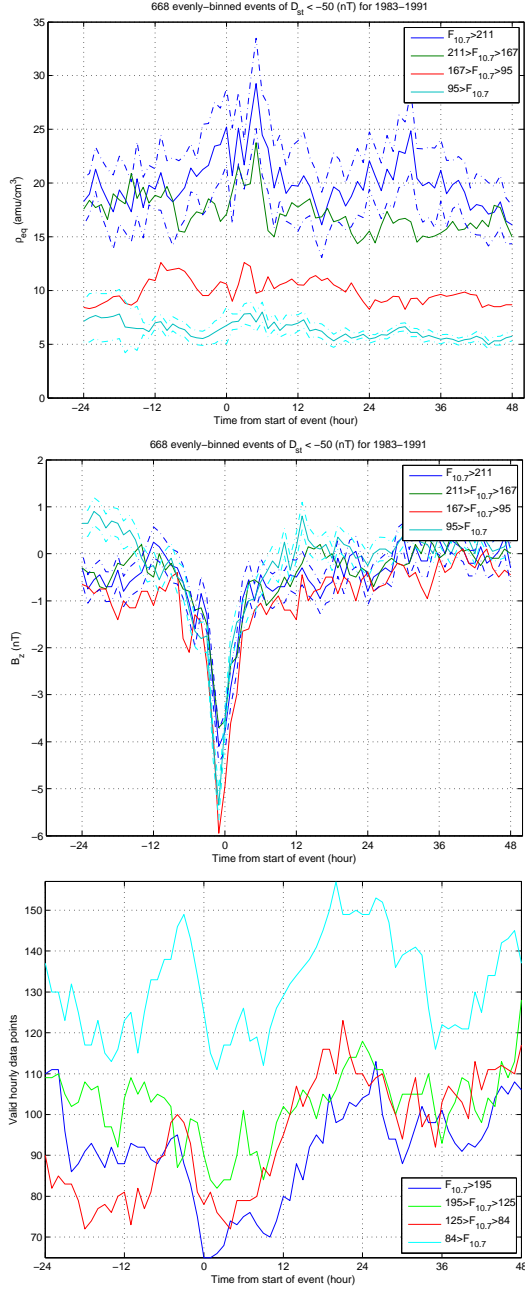
Figure 9: Binning events by $F_{10.7}$ value at onset for ρ_{eq} and, in the middle panel, B_z. Lower panel shows number of valid points in each bin
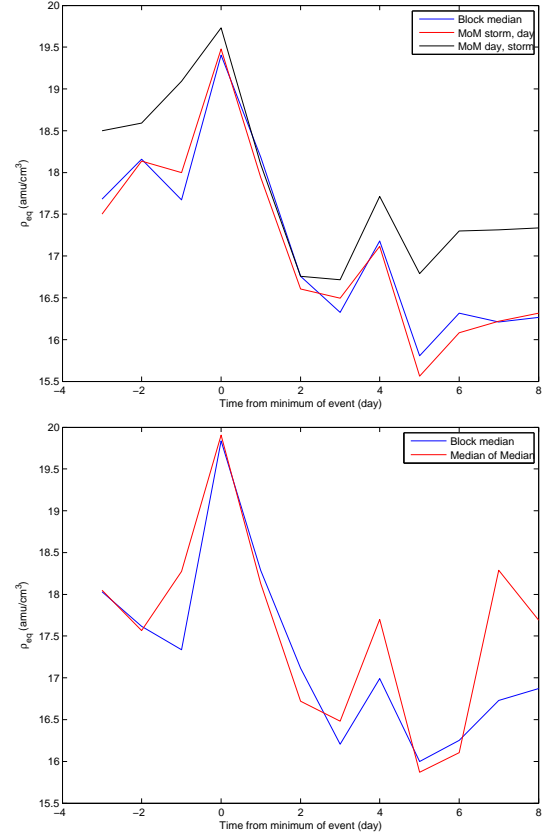
Figure 10: Comparing median values calculated as median of all 1-hour points in the 12 day block, and as the daily median of all hourly-mediated events. (b) Same, but only events starting between 0-12 UTC
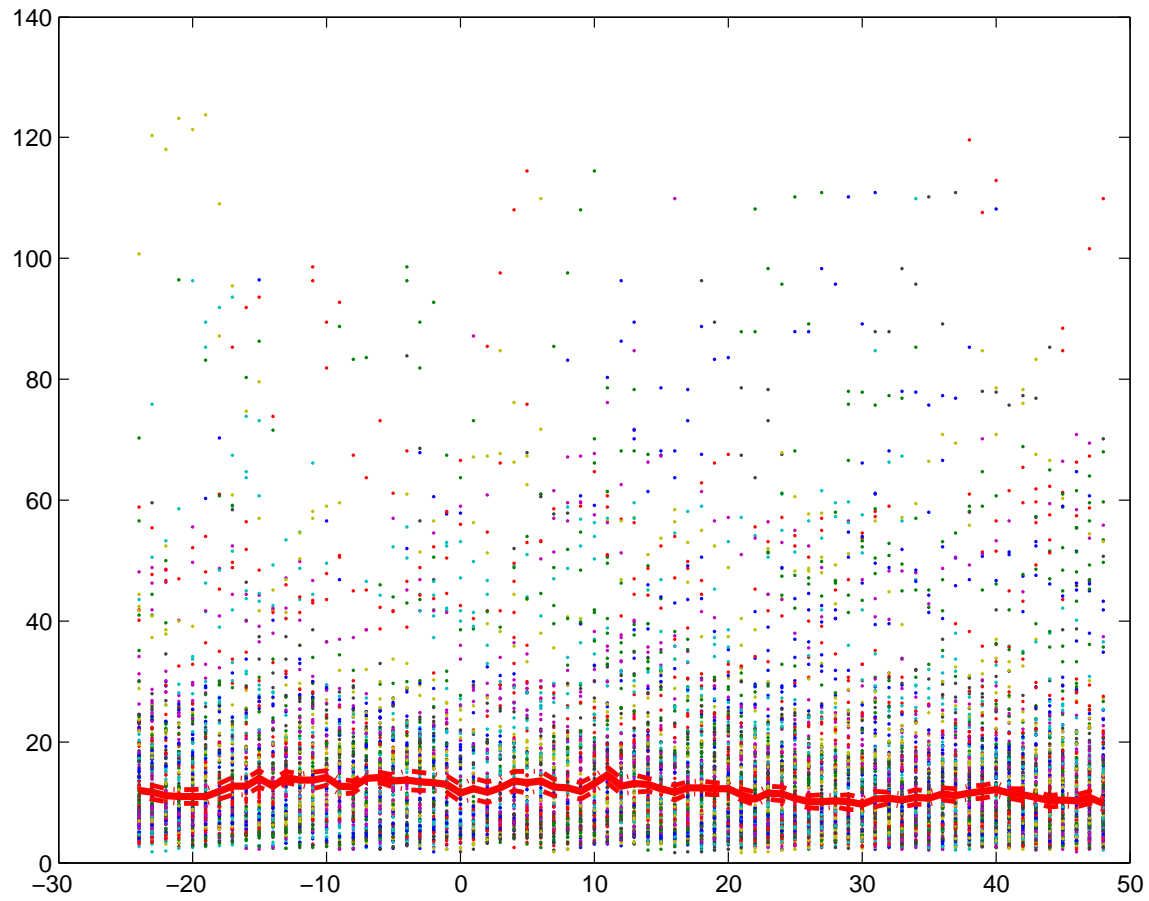
Figure 11: Comparing all events to their median and 1σ range
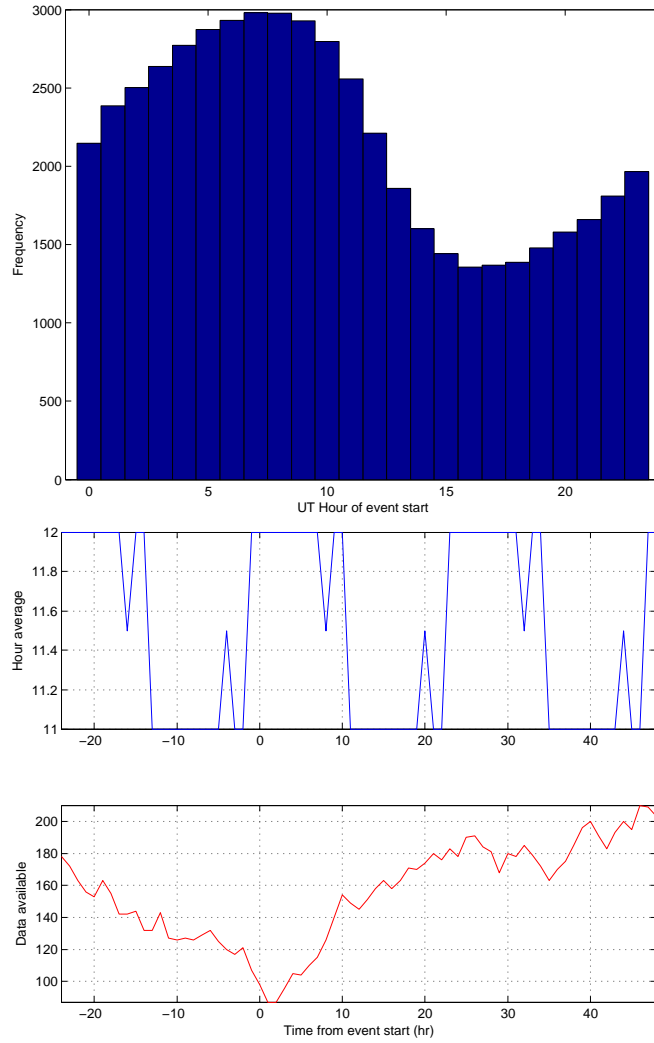
Figure 12: (a) Number of NaN points per hour of observation in the total data set (b) ρ_{eq} data availability relative to average event hour in events where $D_{st} < -80$ nT.

8 Appendix
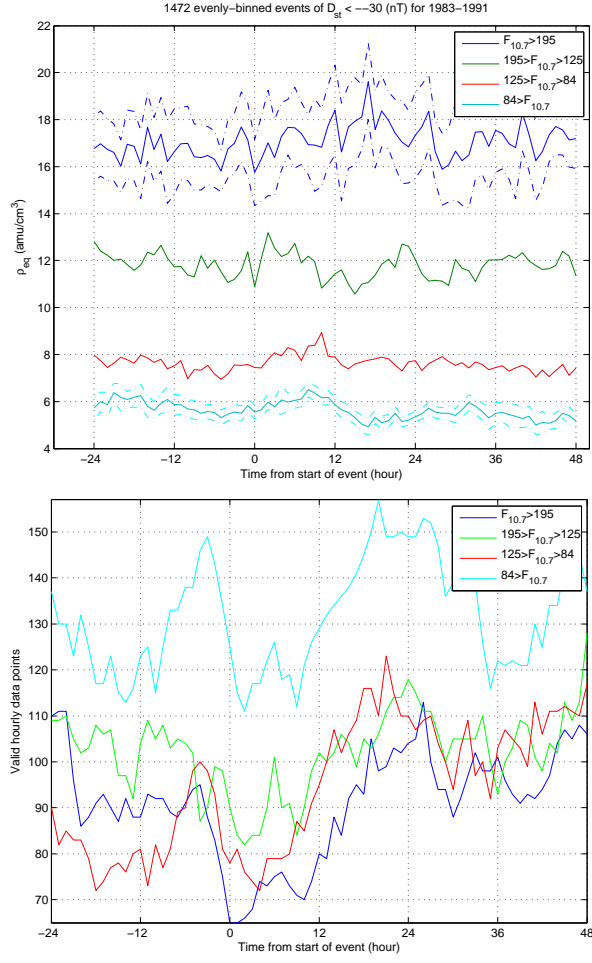
Figure 13: $D_{st} < -30$ nT events, ρ_{eq} binned by $F_{10.7}$. Lower panel: valid hourly points
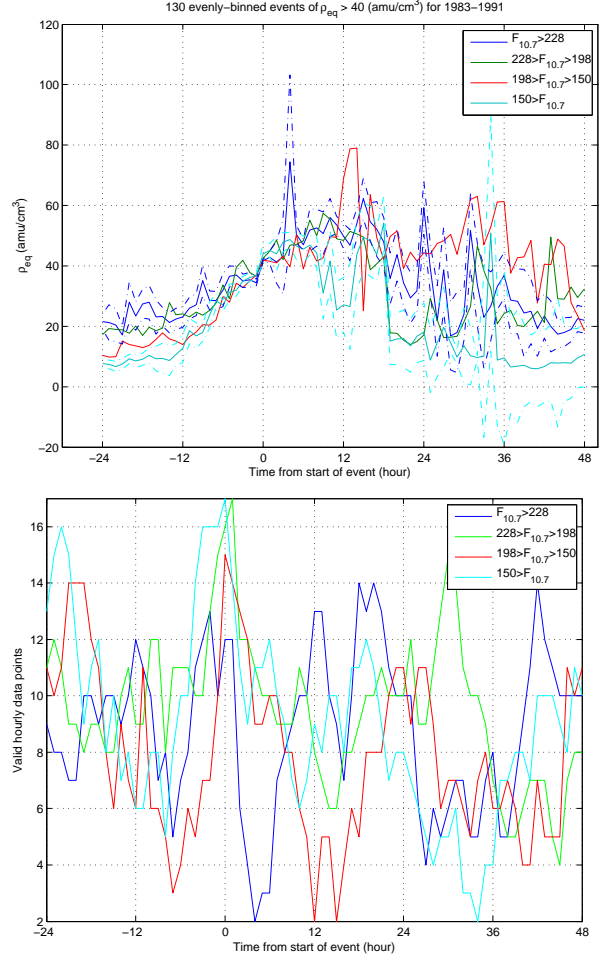
Figure 14: $\rho_{eq} > 40$ amu/cm^3 events, ρ_{eq} binned by $F_{10.7}$
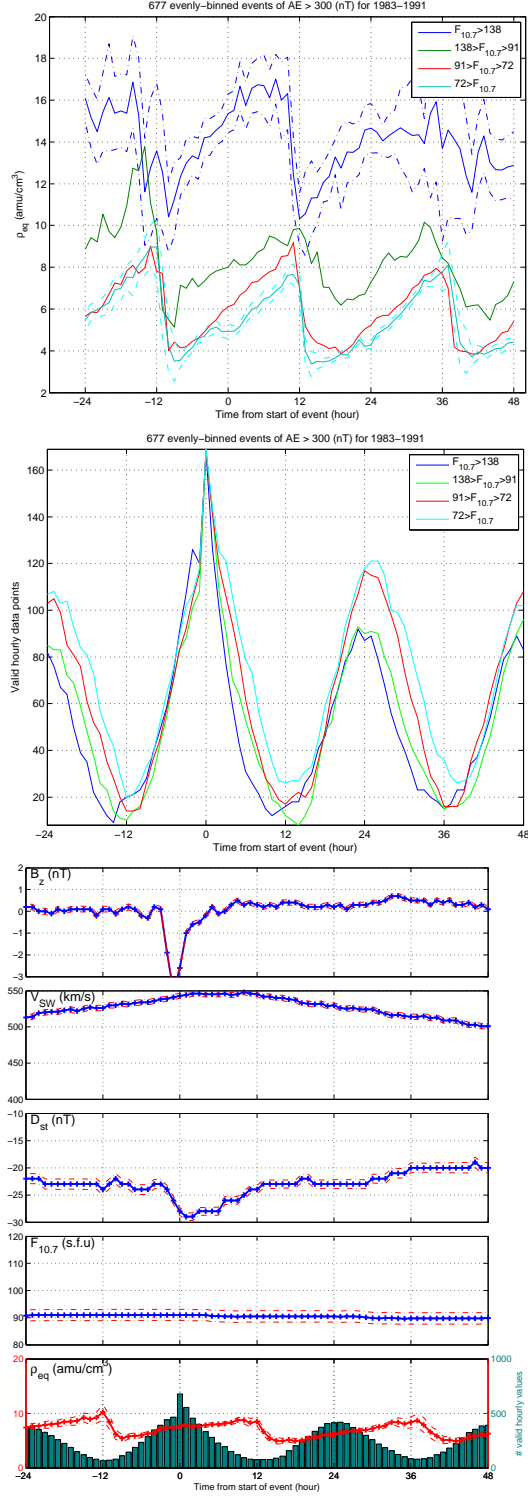
Figure 15: Top: $AE > 400$ nT events, ρ_{eq} binned by $F_{10.7}$ Bottom: averages of $AE > 400$ events
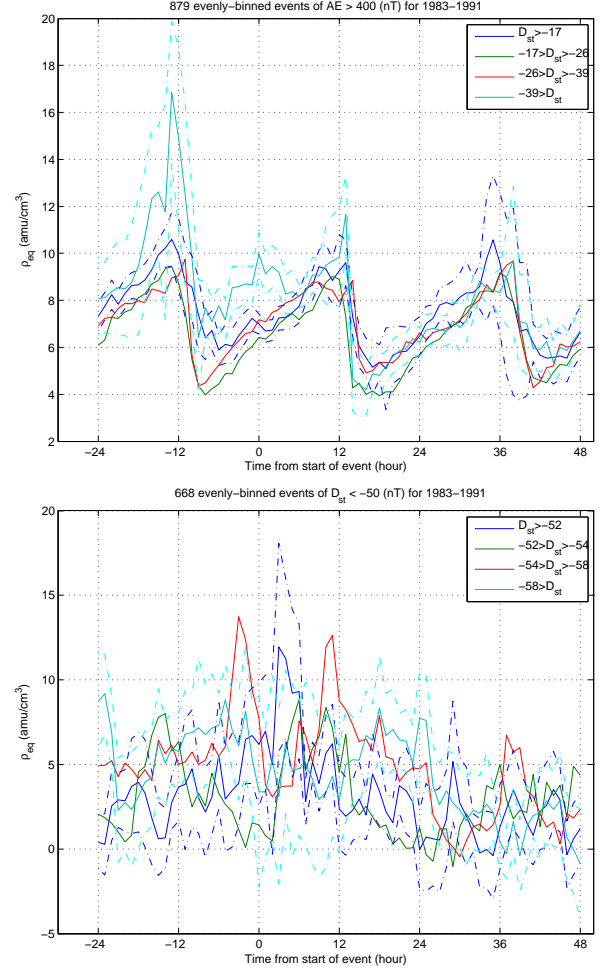
Figure 16: Top: $AE > 400$ nT events. Bottom: $D_{st} < -50$ nT events. Both ρ_{eq} binned by D_{st}.
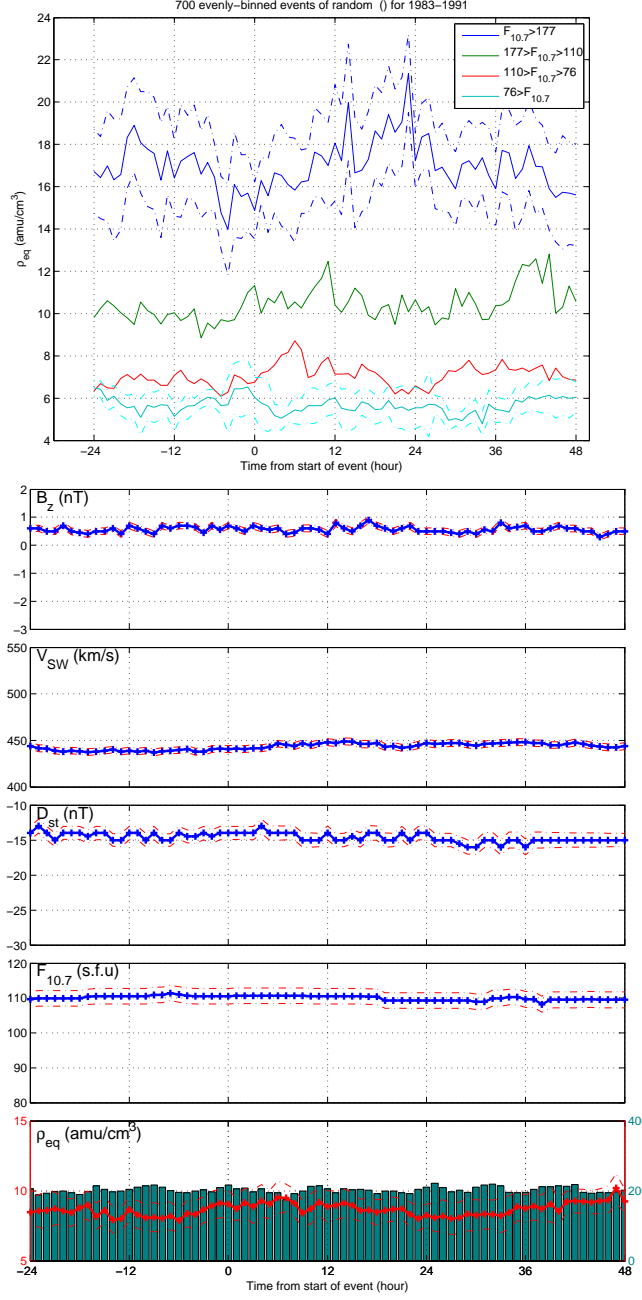
Figure 17: Top: ρ_{eq} binned by $F_{10.7}$ for randomly selected times. Bottom: averages of randomly selected times
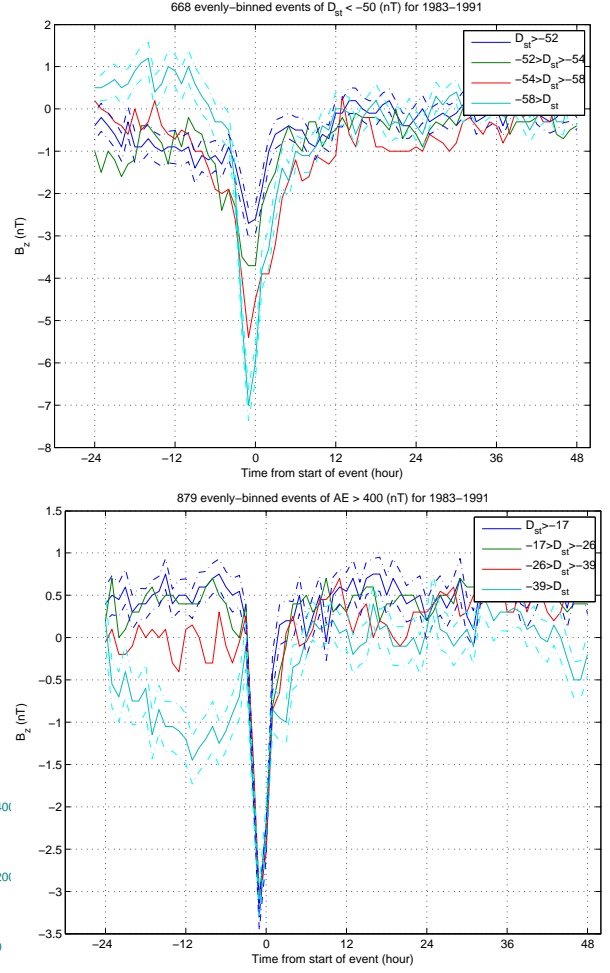
Figure 18: Top: B_z binned by D_{st} for $D_{st} < -50$ nT events. Bottom: B_z binned by D_{st} for $AE > 400$ nT events
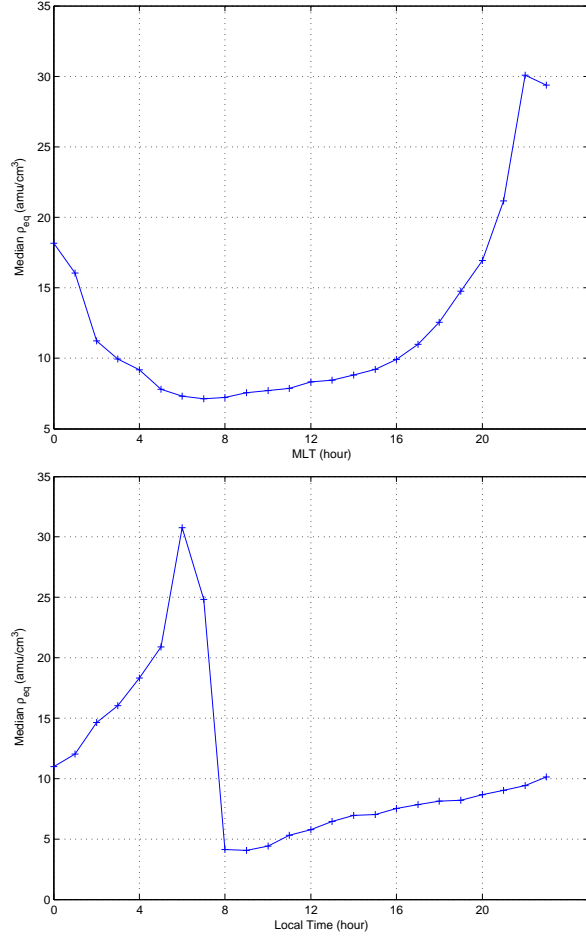
Figure 19: Median ρ_{eq} vs magnetic local time and universal time
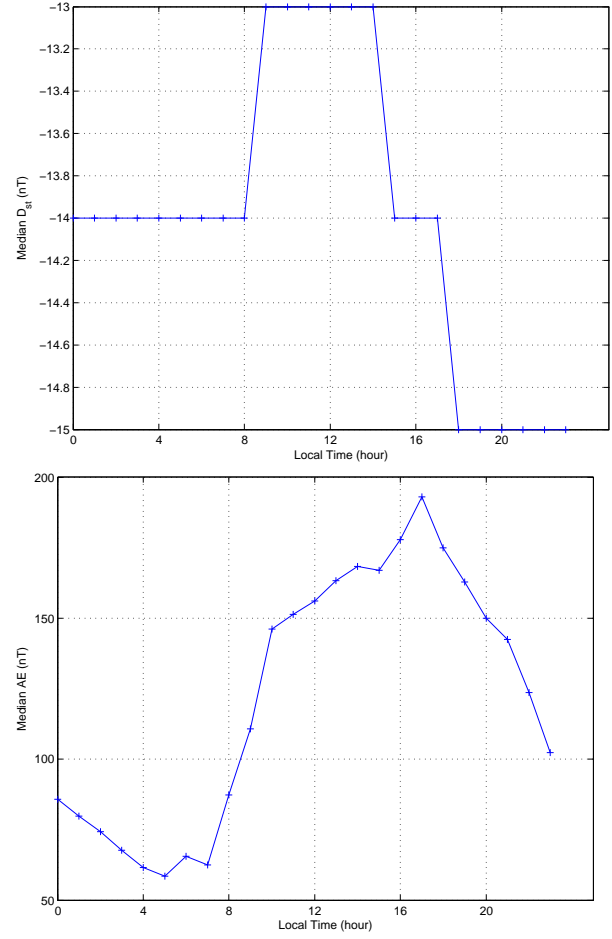
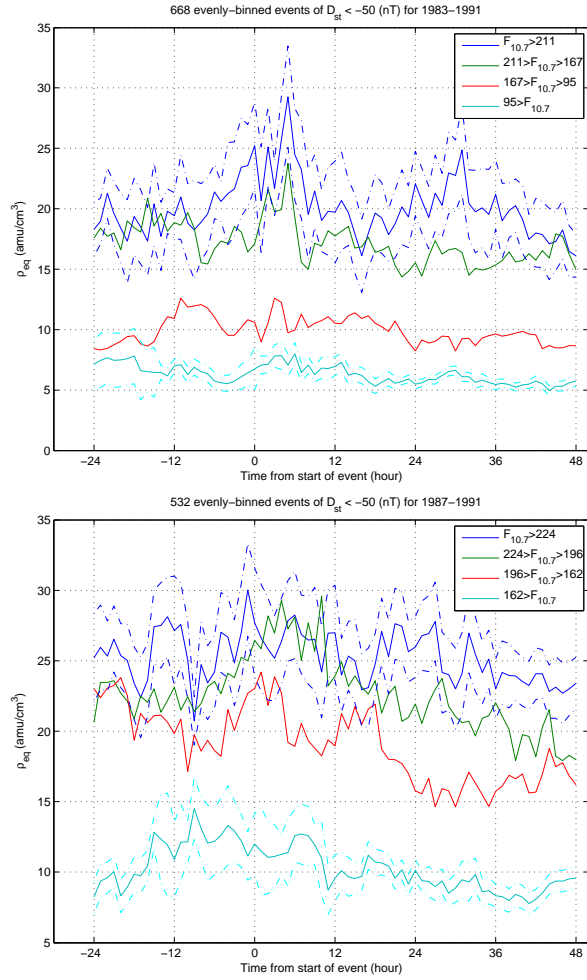Figure 20: Median D_{st} vs universal time, and median AE vs universal time
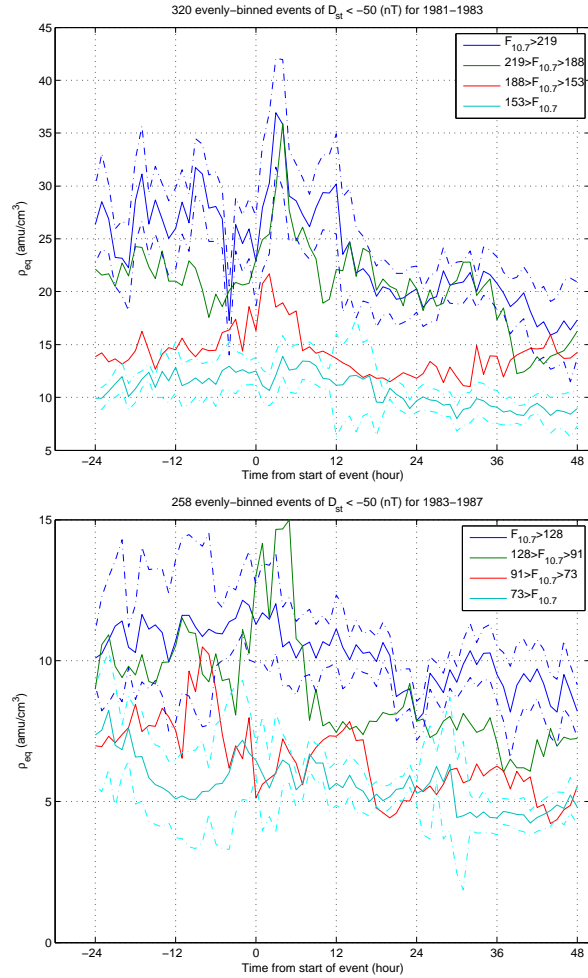
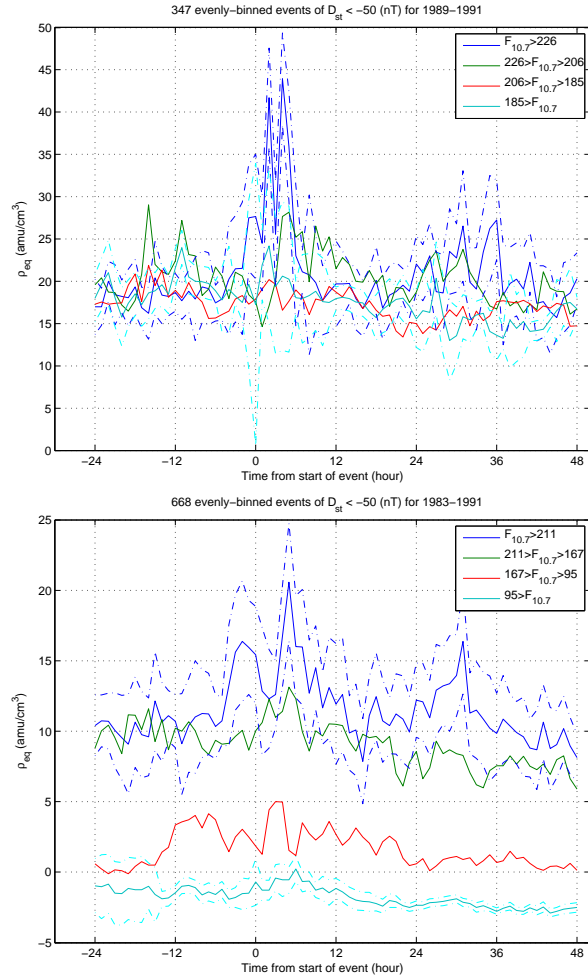Figure 21: GOES Satellite 6 and 7

Figure 22: GOES Satellite 2 and 5

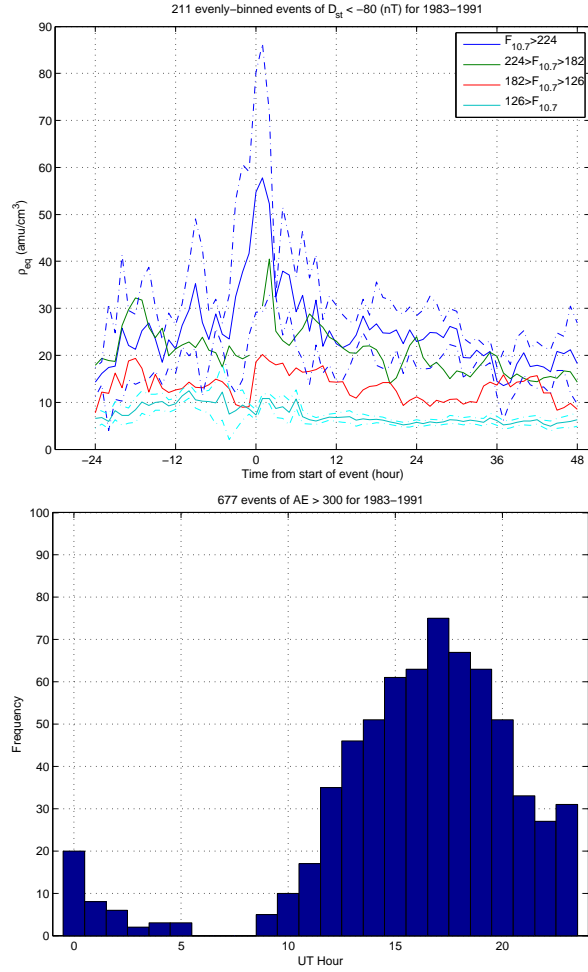Figure 23: Top: From 89-91. Bottom: With ρ_{eq} LT medians subtracted

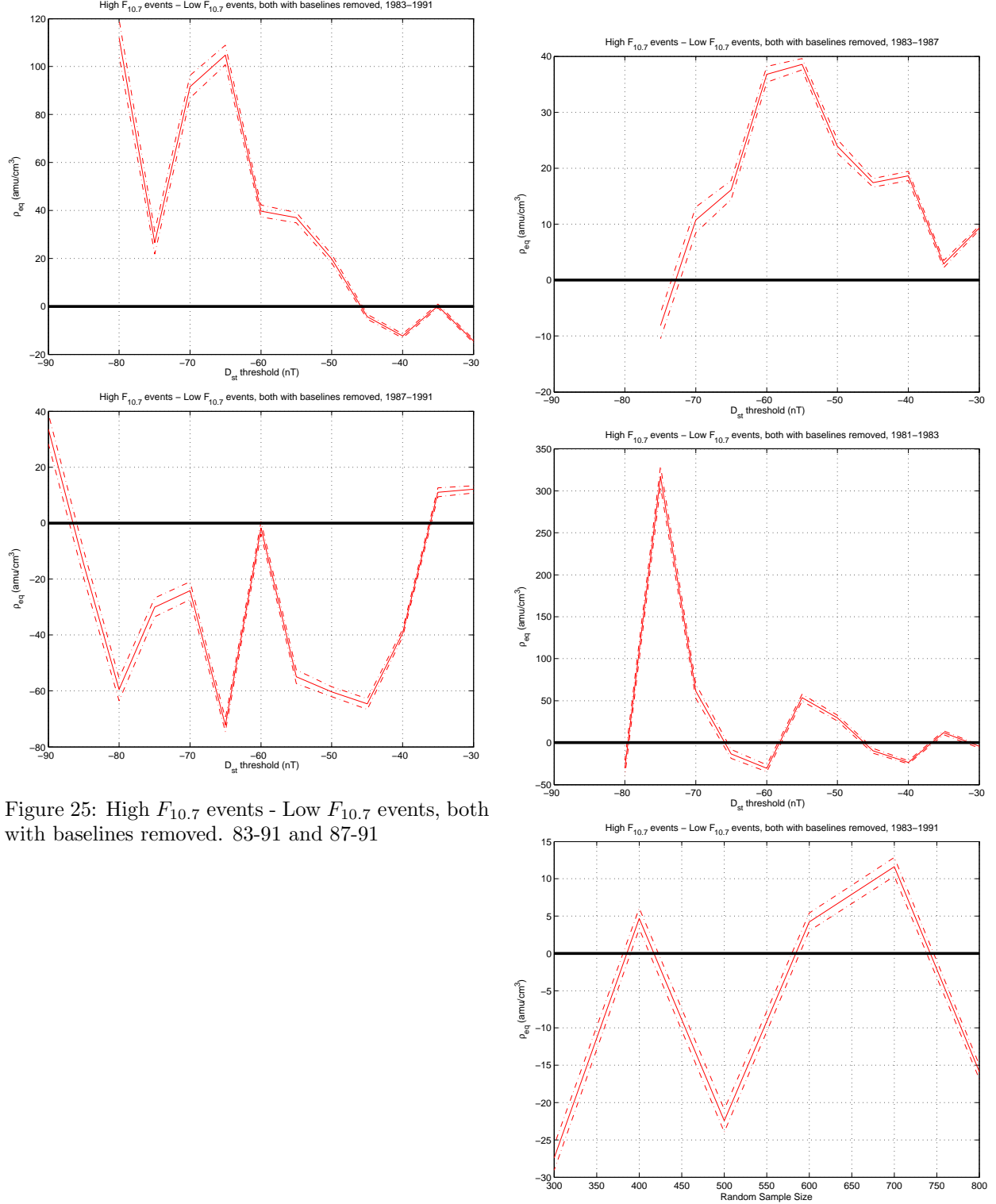Figure 24: Top: $D_{st} < -80$ nT. Bottom: AE events by their hour of onset

Figure 25: High $F_{10.7}$ events - Low $F_{10.7}$ events, both with baselines removed. 83-91 and 87-91

Figure 26: High $F_{10.7}$ events - Low $F_{10.7}$ events, both with baselines removed. 83-87 and 81-83. Bottom: Random "events" from 1983-1991, of sample sizes: 800:-100:300